Journal of Drug Delivery Science and Technology 99 (2024) 105984

Contents lists available at ScienceDirect

Journal of Drug Delivery Science and Technology

journal homepage: www.elsevier.com/locate/jddst

Clay-carvacrol nanoemulsions for wound healing: Design and characterization studies

Anna Imbriano [a], Fatima García-Villén [b], Jacopo Forte [c], Marco Ruggeri [d], Alba Lasalvia [c], Federica Rinaldi [c,*], Luana Perioli [a], Giuseppina Sandri [d], Carlotta Marianecci [c], Cesar Viseras [b,1], Maria Carafa [c,1]

[a] Department of Pharmaceutical Sciences, University of Perugia, Via Del Liceo 1, Perugia, 06123, Italy
[b] Department of Pharmacy and Pharmaceutical Technology, School of Pharmacy, University of Granada, Campus of Cartuja, 18071 S/n, Granada, Spain
[c] Department of Drug Chemistry and Technology, University of Rome "Sapienza", Piazzale A. Moro 5, 00185, Rome, Italy
[d] Department of Drug Sciences, University of Pavia, Viale Taramelli 12, 27100, Pavia, Italy

ARTICLE INFO

Keywords:
Carvacrol
Chitosan
Clay minerals
Nanoemulsions
Wound healing

ABSTRACT

One of the current challenges of scientific research is the design of advanced wound care to obtain a rapid and complete healing of chronic wounds, thus avoiding serious complications. With this purpose, a great deal of attention has been paid to Carvacrol (CRV), a monoterpene and one of the main components of the essential oils of Oregano, Thyme and Satureja Montana. Despite its promising properties in wound treatment, CRV exhibits high lipophilicity, rapid oxidation and volatilization, and inadequate retention time at the site of action, which limit its therapeutic application. A possible technological strategy to overcome these disadvantages could involve the preparation of CRV-based oil in water nanoemulsions (O/W NE) in which CRV itself is used both as the oil phase and as the active compound. CRV-NE uncoated or coated by Chitosan were prepared and deeply characterized. In particular, stability studies were carried out in order to observe some parameters such as dimensions, ζ-Potential, pH and CRV amount at different temperatures over 90 days. Furthermore, the size was evaluated by DLS analyses and compared with data obtained by TEM observations. Secondly, two clay minerals (a montmorillonite and a sepiolite, VHS and PS9 respectively) were added to the NE in order to increase the final viscosity, thus obtaining a semisolid formulation. The rheological properties of the formulations were also studied, in particular, NE and NE-Ch samples were analyzed for 3 months while NE-Ch-VHS, NE-Ch-PS9 for 1 month. Finally, the biocompatibility of CRV-NE, as well as its antioxidant and anti-inflammatory properties, were proved *in vitro* on fibroblasts and macrophages.

1. Introduction

The skin is the wider organ of the human body, and the first line of defense against mechanical, chemical, and biological agents, as well as against ultraviolet radiation. Furthermore, it prevents excessive water loss, regulates body temperature, enhances metabolic functions, and synthesizes vitamin D [1]. The structure of the skin is characterized by the presence of three main epithelial layers: the epidermis, the dermis, and the hypodermis, as well as skin adjuncts (hairs and glands) [2]. Any impairment of the structure and normal functions of the skin could undermine its faculties in protecting the human body from the outer environment. Consequently, the restoration of damaged or altered skin layers becomes essential, a process called “wound healing”. This occurs due to several sequential stages of cellular and biochemical activity known as wound healing that begin after injury and can last for some months [3].

The wound healing is a physiological process that is based on four overlapping specific phases: hemostasis, inflammation, cell proliferation/granulation and remodeling/maturation [4]. According to the mechanism of repair and the time needed to achieve the complete healing, wounds can be classified as acute or chronic [5]. Acute wounds are characterized by the attainment of a complete skin recovery in short periods of time (approximately less than 6 weeks), whereas chronic wounds occur when the healing process does not follow the expected

* Corresponding author.
E-mail address: federica.rinaldi@uniroma1.it (F. Rinaldi).
[1] These authors shared seniorship and they contributed equally.

https://doi.org/10.1016/j.jddst.2024.105984
Received 29 January 2024; Received in revised form 16 July 2024; Accepted 18 July 2024
Available online 21 July 2024

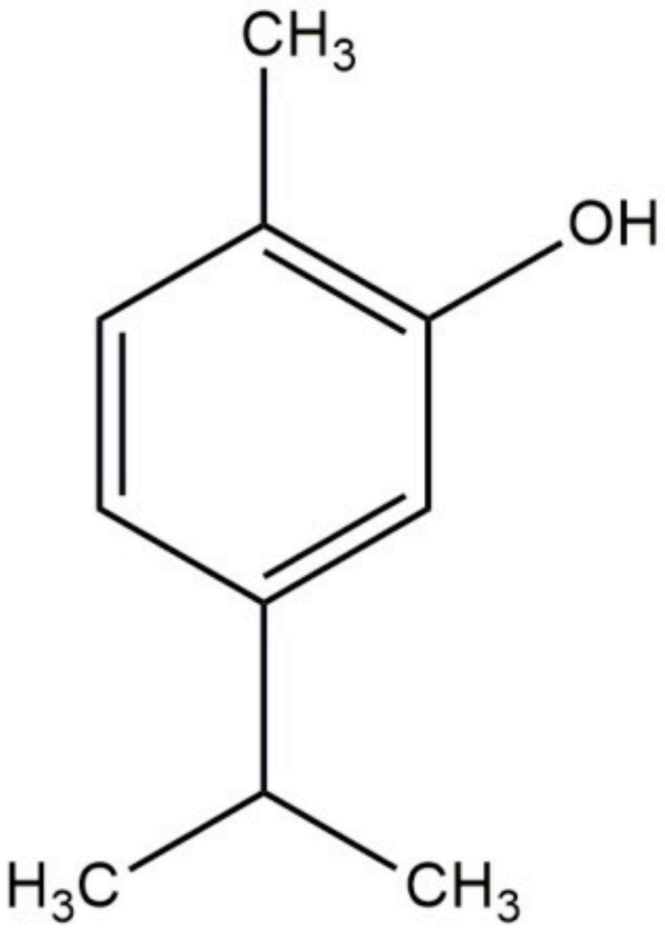

Fig. 1. Chemical structure of Carvacrol.

course, thus not showing significant improvement within 4 weeks or heal completely in 8 weeks or more. Inflammation is the wound healing phase in which a chronic wound usually "stops" [6]. In fact, chronic wounds are frequently aggravated by infections caused by skin and wounds microbiota bacteria that exceed a critical threshold and forms a biofilm, thus exacerbating inflammation and hindering normal wound healing process [7]. Furthermore, a slow and incorrect repair can cause serious damages such as injuries to the circulatory system, and, at worst, the death of the tissue, leading to pain, patient's suffering or even sepsis and, ultimately, to amputation [8].

The current challenge of scientific research is the design of advanced wound care to obtain a rapid and complete healing of chronic wounds avoiding serious complications. With this purpose, a great deal of attention has been paid to several natural compounds with antioxidants, anti-inflammatory, immunomodulatory, and antimicrobial properties useful for the design of wound dressings or other topical formulations. Accordingly, some plant extracts have been successfully employed to promote wound healing [9]. In fact, specific phytoconstituents such as monoterpenes, triterpenes, alkaloids, and polyphenols have shown antioxidant and antimicrobial effects with which they have promoted one or more wound healing processes [10]. Among the natural compounds with these activities, the low molecular weight volatile components of Essential Oils (EO), such as monoterpene and sesquiterpenes, can be mentioned [11]. Carvacrol (CRV) is a monoterpene (Fig. 1) and one of the main components of the *Origanum*, *Thymus* and *Satureja Montana* essential oils; furthermore, it is Generally Recognized as Safe (GRAS) for consumption and approved by the US Food and Drug Administration for food use [12]. CRV has shown specific biological activities which make it an excellent candidate for the development of pharmaceutical products intended for wound repair [13]. In fact, it has been suggested that CRV could act in all phases of wound healing since it shows modulatory effect on the inflammatory cytokines, antioxidant and antimicrobial power, promotion of re-epithelialization, angiogenesis and development of granulation tissue. Finally, it seems to improve the collagen deposition and modulate fibroblasts and keratinocytes proliferation [14]. However, despite its promising biological activities, CRV exhibits high lipophilicity, rapid oxidation and volatilization, hence leading to inadequate retention time at the site of action, which limits its therapeutic application [15].

To solve the physicochemical and biopharmaceutical limitations of essential oils, a possible technological strategy would be represented by CRV based nanoemulsions (NE). Recently, NE have received a great deal of attention from researchers as they present some advantages compared to other drug delivery systems: they are easy to obtain and scalable, they are very effective in promoting the solubilization of active compounds, and they have high permeability and drug loading capacity [16]. NE are very finely dispersed oil-in-water (O/W) or water-in-oil (W/O) emulsions, depending on whether the oil is dispersed as droplets in water, or *vice versa*. In these systems, the small size of the oil or water droplets (nanodroplets) provides better stability to gravitational separation, flocculation, and coalescence with respect to macroemulsions [17]. In the present study we used CRV itself both as the oil phase and as the active compound for the design of O/W NE.

Despite the advantageous properties and characteristics of NE, their low viscosity represents an obstacle for their application over the skin, since it is difficult for liquid formulations to remain over the injured area for enough time [18]. Inorganic excipients such as clay minerals may be used to overcome these problems because they are able to improve technical properties, such as the stability and the viscosity of NE [19]. Furthermore, the clay platelets could be directly pretreated with EO, resulting in the intercalation of oil molecules between the clay galleries and improving their thermal stability. Therefore, although no direct interactions occur in proposed formulation between clays and CRV, NE droplets could be stabilized, from both a thermal and physical point of view, by the presence of clays [20]. Concerning wound healing activity, clay minerals have the ability to physically adsorb and remove microorganisms, toxins, and debris from the wound, thus providing further advantages [21,22]. Clay minerals dispersions in water, at their natural pH (usually is slightly higher than 7), show negative net charged surfaces. This makes them able to interact with positive charged molecules [23]. Bearing this in mind, if the oil droplets, stabilized by surfactant, have a positive surface charge, the clay mineral particles could interact with them, thus establishing intimate electrostatic interaction. Therefore, in this work, to obtain positive charged oil nanodroplets, Low Molecular Weight Chitosan, that is a hydrophilic, mucoadhesive, biocompatible and biodegradable polymer has been used as coating agent. It is widely applied in wound management owing to its hemostatic, stimulation of healing and antimicrobial properties [24]. Due to all the valuable features mentioned above, the coating of the NE with chitosan could facilitate the interaction between NE and clay mineral and it could be useful to enhance both CRV and clay mineral activity in wound healing [25].

Given these premises, the aim of the present research was to design a new pharmaceutical product with potentiated anti-inflammatory, antibacterial and tissue regeneration activity useful in wound healing.

CRV based NE named simply NE, with and without Chitosan, were prepared and fully characterized. In particular, stability studies were carried out monitoring some parameters such as dimensions, ζ-Potential, pH and CRV amount at different temperatures for a period of 90 days. Furthermore, size values obtained by DLS analyses were compared with data obtained by TEM observations. Secondly, two clay minerals were added to the NE to increase the final viscosity, thus obtaining a semisolid formulation. In particular, montmorillonite (with laminar crystal habit) and sepiolite (with fibrous or acicular crystal habits) were used and compared. The resultant rheological properties of the formulations

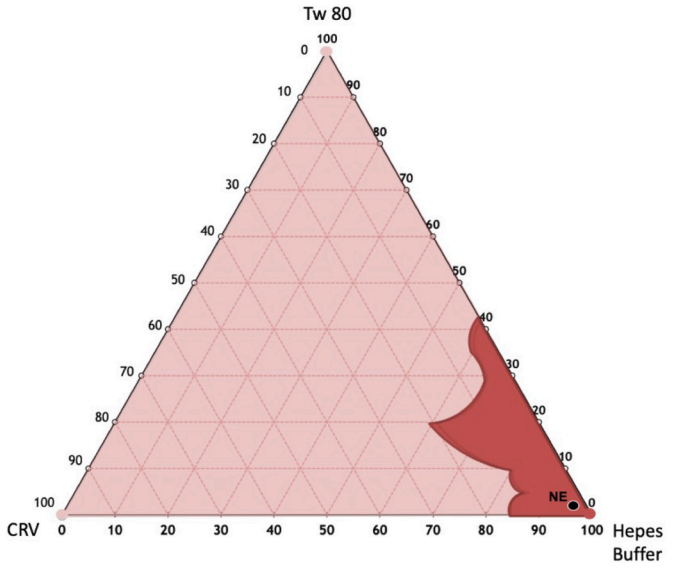

Fig. 2. Ternary phase diagrams among Carvacrol, Tween 80, and Hepes buffer. The observed phases were the homogeneous phase (red area) and the non-homogenous phase (pink area). The formulated nanoemulsion (NE) was selected in the homogeneous region. (For interpretation of the references to colour in this figure legend, the reader is referred to the Web version of this article.)

including clay minerals were also studied. Finally, a biological evaluation of NE was performed considering biocompatibility towards fibroblasts, *in vitro* antioxidant properties, and *in vitro* proinflammatory activity on macrophages.

2. Materials and methods

2.1. Materials

Tween 80 (Tw80), Hepes salt {N-(2hydroxyethyl) piperazine-N-(2-ethanesulphonic acid)}, CRV and Chitosan (low molecular weight, LMW) were purchased from Sigma-Aldrich (Sigma-Aldrich, Milan, Italy). Veegum® HS (VHS) is a pharmaceutical grade montmorillonite, which was kindly gifted by Vanderbilt Company S.A. (USA). Pangel S9 (PS9) is a highly pure sepiolite clay mineral gifted by Tolsa Group company (Madrid, Spain). Purified water was used as the main solvent for all the experiments. All other products and reagents were of analytical grade.

2.2. Hybrid multi-stratified nanoemulsion formulations

2.2.1. Ternary phase diagrams construction

The ternary phase diagram of CRV, Tween 80 and Hepes buffer (pH 7.4) was constructed. The mixtures were prepared by combining appropriate amounts of surfactant, oil phase, and aqueous phase (Hepes buffer). The ingredients were combined at different weight ratios, in a test tube, and kindly mixed to ensure a homogenous mixture of all components. A visual inspection was carried out after each sample preparation to distinguish the monophasic mixture from the biphasic ones. In the ternary diagram, the homogeneous and non-homogenous phase were represented. This study helps to choose the proper amount of each NE constituents selected in the homogenous region.

2.2.2. Hybrid-multi stratified nanoemulsion preparations and chitosan coating

The selected components ratio is reported in the ternary diagram (Fig. 2). Tw80 is a non-ionic surfactant with a hydrophilic-lipophilic balance (HLB) of 15 [26].

Table 1
Samples composition.

Sample	Tw 80 mg/ml	CRV mg/ml	Ch mg/ml	VHS mg/ml	PS9 mg/ml
NE	19.6	9.8	/	/	/
NE-Ch	9.8	4.9	0.5	/	/
NE-Ch-VHS	9.8	4.9	0.5	20.0	/
NE-Ch-PS9	9.8	4.9	0.5	/	100.0

The nanoemulsions were obtained after sonication for 10 min at 25 °C (constant temperature), using a tapered microtip operating at 20 kHz at an amplitude of 20 % (Vibracell-VCX 400, Sonics, Taunton, MA, USA).

In order to obtain Chitosan coated NE, Chitosan LMW (50–150 kDa) was dissolved in acetate buffer (0.2 M, pH 4.4) up to a final concentration of 1 mg/ml and stirred overnight to prepare Chitosan solution. NE and Chitosan solution were mixed at 1:1 ratio [27] and then stirred overnight at room temperature to achieve Chitosan-coated NE (NE-Ch). In conclusion, to confirm the absence of free chitosan in the external phase, a dialysis process was carried out for 24 h using dialysis tube with cut-off 1.000 Da.

Finally, VHS or PS9 were added to NE-Ch under stirring, using a high-speed homogenizer (Ultra Turrax® T25), for 10 min with speed until up 8000 rpm to obtained semi-solid suspensions with a final clay mineral concentration of 2 % w/v.

Table 1 shows the final composition of NE, chitosan coated NE (NE-Ch), chitosan coated NE-Veegum® HS (VHS)/Pangel S9 (PS9) (NE-Ch-VHS, NE-Ch-PS9).

2.3. Dynamic light scattering measurements

Particle size and ζ-potential of NE and NE-Ch were determined by dynamic light scattering (DLS) by means of a Zetasizer Nano-ZS90 (Malvern Instruments, Worcestershire, UK), equipped with a 5 mW HeNe laser (wavelength $\lambda = 632.8$ nm) and a digital logarithmic correlator. The measurements were carried out at a fixed angle of 173°, at 25 °C. The particle size of CRV nanodoplets was described by the cumulants mean diameter (Z-Ave) and the size distribution was described by the polydispersity index (PDI). Specifically, a PDI value $\leq$ 0.3 indicates a homogenous population of particles [28]. ζ-potential measurements were conducted by the same instruments (Zetasizer Nano-ZS90), which determined the ζ-potential (ζ-Pot) of NE, NE-Ch, NE-Ch-VHS and NE-Ch-PS9 by measuring the direction and velocity of emulsion in an applied electric field. The Z-Ave, PDI and the ζ-Pot were calculated as the average of three measurements. DLS measurements were also utilized for the "Dilution Test". NEs were diluted with double-distilled water and visually inspected for cracking, phase separation, and clarity or turbidity. Additionally, both undiluted and diluted NEs (at 1:10, 1:50, 1:100, 1:500, 1:1000, and 1:10000 ratios) were analyzed by Dynamic Light Scattering method.

2.4. Stability studies

2.4.1. Long-term stability studies

Stability studies of NE and NE-Ch were carried out by monitoring the Z-Ave and ζ-pot with time, by a Zetasizer Nano-ZS90 instrument, working under the same conditions as previously described. The samples were stored at 4 °C and 25 °C for 90 days and the measurements have been carried out at predefined time intervals (1, 30, 60 and 90 days).

2.4.2. CRV decomposition/degradation studies

To assess the stability of CRV in terms of decomposition/degradation within the formulations, the CRV solution (CRV solubilized in a mixture of Ethanol:Hepes 50:50 (vol:vol)), NE and NE-Ch were analyzed [29].

Each sample was examined using a UV spectrophotometer (PerkinElmer, Lambda 25) to determine the CRV absorbance peak at 273 nm immediately (after sample preparation) and at different intervals (1 day, 30 days, and 60 days), with samples maintained at 25 °C and 4 °C [30]. Similarly, also CRV stability was evaluated before and after sample preparation using the sonication method where temperatures exceed room temperature. To demonstrate that the temperature does not affect the CRV stability, mass spectrometric analyses were performed, according to the following procedure: a small volume (200 μL) of two aliquots of NEs (before and after sonication) were filtered through a 0.45 μm syringe filter (Merck Millipore, Darmstadt, Germany) to remove particulates. Then, 1 μL of each filtered solution was diluted in methanol (Sigma Aldrich, MS grade) to obtain a final concentration of 0.1 mg/L. These solutions were directly injected in the electrospray source (ESI) and analyzed in negative ionization mode (ESI(−)). The analyses were performed by using a Linear Ion Trap mass spectrometer (LTQ XL, Thermo Fisher, Waltham, MA, USA). The spectra were recorded in the mass range between m/z 50–500 and the flow rate was set to 10 μL/min; other parameters were: capillary temperature at 250 °C, capillary voltage at −50 (V) and tube lens at −121 (V).

2.4.3. Centrifugation test

The samples NE, NE-Ch, NE-Ch-VHS and NE-Ch-PS9 were centrifuged for 30 min at 3000 rpm and 25 °C. All samples were visually inspected to evaluate eventually creaming and phase separation [31, 32], while only NE and NE-Ch have been also analyzed by DLS measurements.

2.5. Transmission Electron Microscopy

The formulations were analyzed by Transmission Electron Microscopy (TEM) technique. Diluted samples (1:10 to 1:50) were placed over a SiO_2 copper grid (200 mesh) for a negative staining with uranyl acetate (1 %, pH 7). The nanoemulsions were observed under a Libra 120 PLUS (Carl Zeiss, Weimar, Germany) equipped with EELS (resolution <1.5 eV).

2.6. Rheology

The rheological properties of the formulations were determined with a RotoVisco™ 1 (Thermo Scientific™ HAAKE™, Massachusetts, US) equipped with a plate/cone combination (2°, Ø 60 mm). Rheological properties of the formulations were measured between 70 and 800 s^{-1}. The rheological measurements consist of flow curves performed at 32 °C (±0.5 °C, human skin temperature) between 70 and 800 s^{-1} to study the rheological behaviour of the samples from their recipient, through topical administration to high shear rates. Moreover, the flow curves were obtained at predetermined times after samples preparation in order to monitor the time-stability and possible interactions between ingredients that could lead to rheological modifications. Three replicates were obtained for each sample and data were processed by the HAAKE RheoWin software. Rheological characterization included flow curves, apparent viscosity taken from the upper flow curve at 250 s^{-1} and hysteresis area. The hysteresis area was obtained by measuring the area-under-the-curve of each flow curve. More particularly, the rheology of NE and NE-Ch samples was analyzed for 3 months in order to monitor possible time changes within the formulation within this period. NE-Ch-VHS, NE-Ch-PS9 were also measured (for 1 month). To study the effect of each clay mineral in combination with NE and NE-Ch, VHS and PS9 were dispersed (at the same concentration) in acetate buffer, samples also monitored in terms of rheology (VHS-buffer and PS9-buffer).

2.7. pH analysis

pH values of all samples were evaluated using a pH meter (pH25+, Hach Lange, Berlin, Germany) equipped with a semisolid 5053T electrode. The pH of each sample was measured in sextuplicate, without previous dilution immediately after sample preparation.

2.8. In vitro cell studies

2.8.1. Cytotoxicity and fibroblasts morphology

The cytotoxicity of the samples was assessed using Normal Human Dermal Fibroblasts (NHDFs). NHDFs were grown in Dulbecco's modified Eagle medium (DMEM, Sigma-Aldrich, Italy) supplemented with 10 % v/v fetal bovine serum (FBS, Euroclone, Italy), and penicillin/streptomycin solution (pen/strep, 100 UI/100 μg/mL, Sigma-Aldrich, Italy). Normal culture conditions take place at 37 °C in a 5 % CO_2 atmosphere with 95 % relative humidity. Briefly, cells were seeded onto 96-well at a density of 35,000 cells/well and grown until 80 % confluence in a monolayer (24 h). Before the analysis, each sample was suspended in a serum-free DMEM (dilutions 1:10, 1:100, 1:200) and added to the wells seeded with confluent cells. After 24 h of sample and cell contact, the viability of cells was assessed using Alamar Blue™ (Thermo Fisher Scientific, Italy) assay. To do so, the growth medium containing samples was removed, and 100 μL of a AlamarBlue solution (10 % w/w in DMEM w/o phenol red) were placed in each well. The well plate was incubated at 37 °C for 3 h, before fluorescence reading in a FLUOstar® Omega Microplate Reader.

Moreover, the morphology of fibroblasts after 24 h of contact with the samples was investigated using confocal laser scanning microscopy (CLSM) after nuclei and cytoskeleton staining. Cells were plated onto glass slides in a 24-well plated at a density of 70,000 cells/well. One 80 % confluence was reached, the samples (dilution 1:200) were added to the plate and incubated for 24 h. After this period the cells grown onto glass slides were fixed with 4 % glutaraldehyde solution for 15 min and washed with PBS. Then, the cytoskeletons were stained with FITC Atto 488 phalloidin (50 μL at 20 μg/mL in PBS in each well, contact time 30 min), while with Hoechst 33,258 was used to stain the nuclei (100 μL at 1:10.000 dilution in PBS per each well, contact time 10 min in the dark) (Sigma-Aldrich, Milan, Italy). Finally, the slides were visualized in a CLSM (Leica TCS SP2, Leica Microsystems, Milan, Italy) working at λ_{ex} 346 nm and λ_{em} 460 nm for Hoechst 33,258 and λex 501 nm and λem 523 nm for FITC-phalloidin.

2.8.2. Assessment of antioxidant properties

The antioxidant properties of the formulations were also evaluated on NHDF. The concentration of H_2O_2 necessary to induce a proper oxidative damage, without leading to a complete cell death, was identified as follows. Cells were seeded onto 96-well at a density of 35,000 cells/well, grown until 80 % confluence in a monolayer (24 h), and put in contact with different concentrations of hydrogen peroxide (H_2O_2) in a serum-free DMEM (from 0.5 to 3 mM). After 3 h of contact, the Alamar Blue™ assay was conducted to determine cell viability, as previously described.

Thereafter, cells (35,000 cells/well) were pre-treated with the samples (dilution 1:200) for 24 h, and then, with 1.15 mM H_2O_2 for another 3 h. Finally, the AlamarBlue™ assay was conducted to determine cell viability.

2.8.3. Biocompatibility and anti-inflammatory properties on macrophages

Raw 264.7 murine macrophage cells were cultured in DMEM supplemented with 10 % v/v FBS, and with penicillin/streptomycin solution (pen/strep, 100 UI/100 μg/mL), under the same conditions described in previous sections. Cells were plated onto 96-well (35000 cells/well) and grown until 80 % confluence in a monolayer (24 h). Each sample was suspended in a serum-free DMEM (dilution 1:10, 1:100, 1:200) and added to the wells, letting them in contact with cells for 24 h. Then, the cytocompatibility was assessed with MTT (3-(4,5-dimethylthiazol-2-yl)-2,5-diphenyltetrazolium bromide, Sigma-Aldrich, Italy). At this purpose, the culture medium and samples were

Table 2
Hydrodynamic Diameter (HD), ζ-Potential (ζ-Pot), polydispersity index (PdI) of NE and NE-Ch. Values represent the mean ± standard deviation of n = 3 NE sample measurements.

Sample	Z Ave (nm) ± SD	ζ-Pot (mV) ± SD	PdI ± SD
NE	135.60 ± 0.75	−13.30 ± 1.45	0.21 ± 0.03
NE-Ch	225.10 ± 0.98	13.6 ± 1.00	0.15 ± 0.01

withdrawn from the wells and 100 μl of MTT solution (1 mg/ml solubilized in DMEM w/o red phenol) were added. Afterwards, 100 μL of isopropanol were put in each well and the absorbance was read at 570 nm.

Thereafter, cells (35,000 cells/well) were pre-treated with the samples (dilution 1:200) for 24 h, followed by lipopolysaccharide (1 μg/ml) for another 3 h. Untreated cells (without samples) subjected to LPS-inflammation were considered as the negative control (LPS), while untreated cells without LPS-inflammation (GM) acted as positive control. Finally, the MTT assay was performed to determine cell viability.

3. Results and discussion

3.1. Formulation and characterization of hybrid-multistratified nanoemulsion

The ternary phase diagram of CRV, Tw80 and Hepes buffer (aqueous phase) was developed, and homogeneous/nonhomogeneous phase regions were identified, enabling the selection of the appropriate formulation.

The homogeneous region is highlighted in red. From the red region, specific sample has been selected to obtain a final formulation with no toxicity profile. In particular, the surfactant concentration has been chosen to simultaneously stabilize the oil nanodroplets in water and to guarantee no irritating/side effects [33,34].

The ternary diagram (Fig. 2) shows the selected formulation (the composition is shown in Table 1).

The biological efficiency, drug delivery, penetrability, and cellular response of the NE could depend on their physicochemical characteristics including average diameter, PDI and stability, among other parameters [35]. However, the droplet size does not represent a fundamental parameter regarding wound healing because the injured and inflamed skin can also be treated by particles larger than the nanoscale due to the integrity loss of the *stratum corneum* and its barrier function [36,37]. NE and Ch-NE were prepared as described in section 2.2 and their Hydrodynamic Diameter (HD), ζ-Potential (ζ-Pot), polydispersity index (PdI), pH values have been reported in Table 2. NE shows a mean HD around 130 nm while a higher HD value was observed after Ch coating (NE-Ch HD = 225 nm). Both samples were homogeneous, without evidence of clump formation, creaming or flocculation.

The bigger dimensions of NE-Ch confirm that Ch surface coating was successful. This result was further confirmed by ζ-Pot analyses: a negative charge was reported for NE (−13.3 mV), which was inverted to positive value after chitosan coating in NE-Ch [38]. Furthermore, DLS analysis did not detect any particles exhibiting micelle-like size and morphology. To verify these features, we included in the Supplementary Information (Figs. S1, S2, and S3) the distributions of intensity, volume, and number from the DLS analyses, which confirm, together with TEM analyses, the presence of only NEs and the absence of micelles.

PdI values of both samples were of 0.2 or below; it means that our formulations are characterized by a homogenous nanodroplets population.

In addition, to confirm that the proposed nanocarriers were indeed nanoemulsions, a "Dilution Test" was performed. NEs were diluted with double-distilled water at various ratios (1:10, 1:50, 1:100, 1:500, 1:1000, 1:10000) and they were visually examined for cracking or phase separation and by DLS. The results, presented in the Supplementary Information (Table S1), show the hydrodynamic diameter (HD) and ζ-potential (ζ-Pot). The features of the samples analyzed remained the same before and after dilution, with no observed cracking or phase separation. These results confirm the formation of NEs.

3.2. Hybrid-multistratified nanoemulsion stability evaluation

Stability evaluation is a crucial step for any drug delivery system. It is a productive and proactive step to consider the stability of the nanocarriers during the early formulation design as well as after their preparation since the product should maintain its physical and chemical

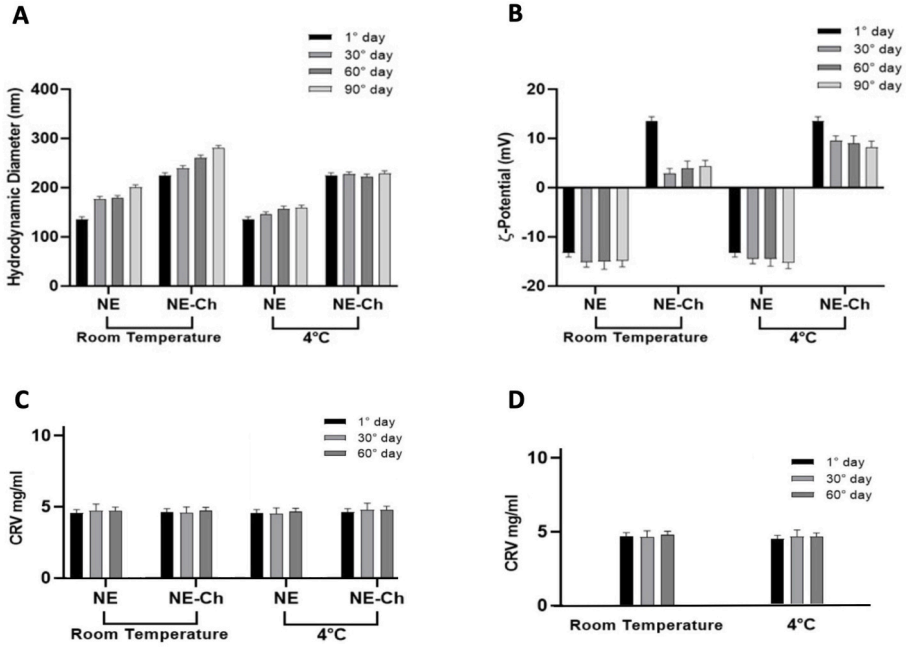

Fig. 3. Physical stability studies in terms of hydrodynamic diameter (A), ζ-potential (B), and CRV content (C and D) variations of uncoated (NE) and of Ch coated nanoemulsions (Ch-NE) up to 90 days at two different storage temperatures (* = $p < 0.05$ when compared with day 1).

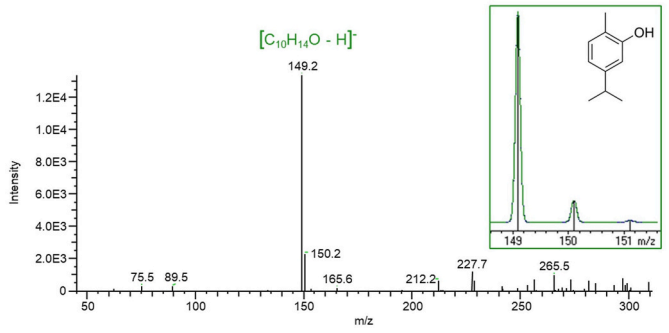

Fig. 4. Enlargement of ESI (−) MS spectrum and theoretical pattern (shown in green panel) of carvacrol [C10H14O–H]- at *m/z* 149 as detected in standard solution. (For interpretation of the references to colour in this figure legend, the reader is referred to the Web version of this article.)

integrity during storage and until their use.

In order to obtain information about the main factors inducing changes on their properties (Z-Ave, ζ-potential, and CRV content), the physical-chemical stability of NE and NE-Ch was evaluated under different environmental conditions. Both samples were stored for 3 months at two different temperatures. It is well known that NE are not thermodynamically but kinetically stable systems and for this reason they could suffer long term instability phenomena such as creaming, sedimentation, flocculation, coalescence, Ostwald ripening and finally phase separation [39–41]. Among them, Ostwald ripening and coalescence are the most frequent, both characterized by the union of smaller droplets into bigger ones that are energetically favored [42]. These phenomena are probably influenced by temperature as shown in Fig. 3, panel A. In particular, it is possible to state that NE and NE-Ch stored at 4 °C were stable in terms of size and ζ-potential, while at RT their hydrodynamic diameter significatively increased during the experiment (Fig. 3, panel A and panel B). Probably, the dispersed vesicle stability was affected by temperature and ζ-potential values. In particular, the colloidal dimensions of samples maintained at 4 °C were constant because of the reduced collision events between dispersed vesicles. At RT, the collision phenomena are more significant, and the ζ-potential of each sample (−13.3 mV and +13.6 mV for NE and NE-Ch respectively) doesn't preserve the sample by coalescence phenomena with consequent size increasing [43]. In fact, the ζ-potential value necessary to assure good time stability is higher with the respect to ± |30 mV| [44] because this ζ-potential value can enhance repulsion effects to prevent aggregation, precipitation phenomena or in general instability phenomena such as creaming, sedimentation, flocculation. Stability studies of CRV (both free and encapsulated in NEs) were conducted using UV analysis as described M&M. In particular, the CRV content in NEs and the NE-Ch were compared to free CRV, and the obtained result were shown in Fig. 3, Panel C and Panel D. It was observed that CRV content remained stable throughout the experiment at both 25 °C and 4 °C, indicating that other NE components (surfactant and Ch) did not affect the CRV stability.

To ensure that CRV absorbance is not hindered by other formulation components, the UV peak of free CRV and CRV structured in NEs is displayed in Fig. S4. CRV degradation profile and its content in NE were also investigated by means of mass spectrometry (MS). The preparation method involving high-intensity ultrasonic waves can raise sample temperatures up to 60 °C. Given the volatility of CRV, it was necessary to assess its composition before and after sample preparation by MS.

A preliminary analysis was performed by injecting a standard methanol solution of carvacrol (0.1 mg/L), thus revealing its deprotonated ion, $[C_{10}H_{14}O–H]^-$, at *m/z* 149, as shown in Fig. 4. After preliminary tuning, pre- and post-sonicated suspensions were injected in the mass spectrometer under the same operative conditions, thus revealing the presence of the peak *m/z* 149 and showing a high stability

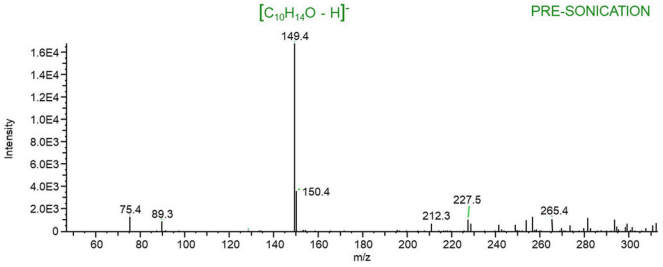

Fig. 5. Enlargement of ESI (−) MS spectrum of carvacrol [C10H14O–H]- at *m/z* 149 in the pre-sonication solution.

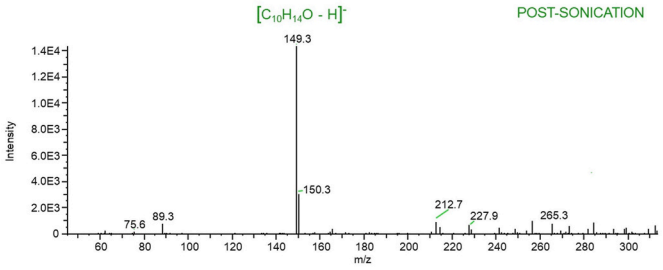

Fig. 6. Enlargement of ESI (−) MS spectrum of carvacrol [C10H14O–H]- at *m/z* 149 in the post-sonication solution.

even above 60 °C. Both spectra are displayed in Fig. 5 (pre-sonication) and Fig. 6 (post-sonication). These results suggest that the temperature does not affect the CRV stability and confirm the obtained storage results carried out by UV measurements.

3.2.1. *Centrifugation test*

To obtain more information about stability and speed up the potential destabilization process, each sample was subjected to mechanical stress using the centrifugation method as described in paragraph 2.4.3. At the end of the cycle (3000 rpm, 30 min, room temperature), NE, NE-Ch, NE-Ch-VHS and NE-Ch-PS9 formulations were analyzed and compared.

NE and NE-Ch maintained their initial characteristics and no instability phenomena were observed. Furthermore, both samples were analyzed by DLS in order to observe possible variations of size, ζ-potential or PdI, but no changes were detected.

On the other hand, the formulations NE-Ch-VHS and NE-Ch-PS9 showed to release water after centrifugation, but no free oil was found. Potential water syneresis in VHS systems may be reduced by simultaneous adsorption of water molecules in the clay mineral interlayer, whereas in PS9, a non-laminar and, therefore, a not swelling clay mineral, this attenuation effect is not possible. In particular, for the sample NE-Ch-PS9 the height of free water after centrifugation was larger than for NE-Ch-VHS. This is likely an effect due to the higher viscosity of the sample obtained with the addition of the VHS compared to the addition of PS9.

Despite the presence of a small fraction of free water, the obtained results in the NE suggest that both samples formed a relatively stable network in which the oil droplets were trapped.

3.3. *Transmission Electron Microscopy*

Regarding the morphology, structure and particle size of the NE and the NE with clays, the four samples (NE, NE-Ch, NE-Ch-VHS and NE-Ch-PS9) were investigated by TEM. Fig. 7 (panel A and B) reveals that all the droplets in the nanoemulsions were almost spherical in shape and confirmed the dimension range obtained by DLS. It appears, as is well known, that NE with spherical morphology can disperse well without

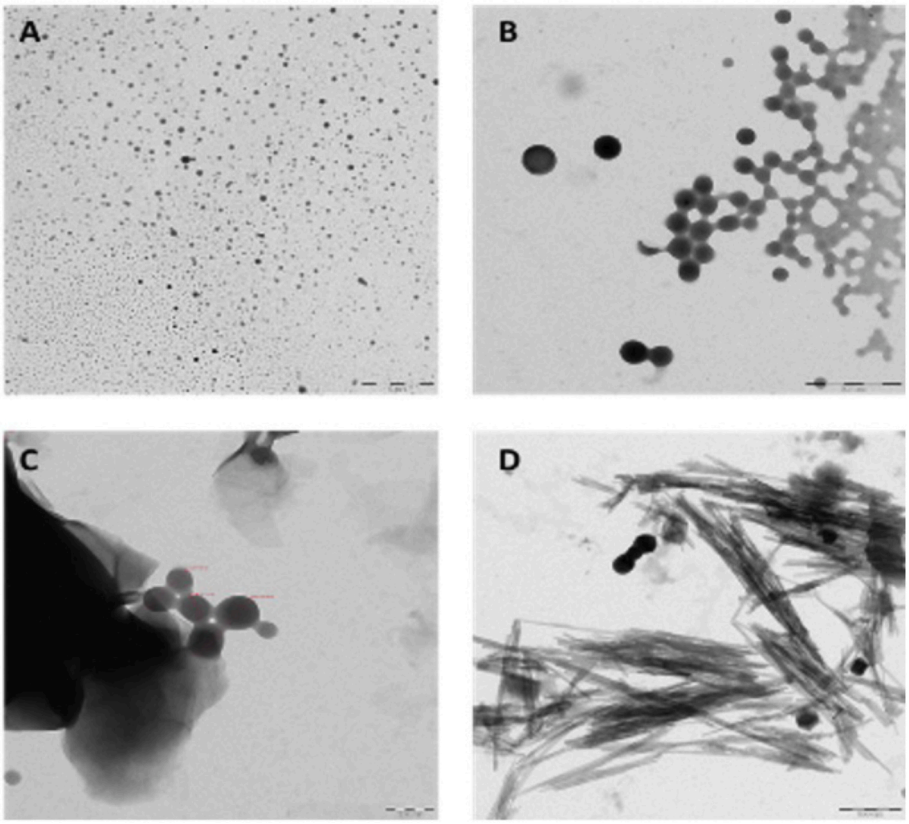

Fig. 7. TEM microphotograph of NE (A), NE-Ch (B), NE-Ch-VHS (C), NE-Ch-PS9 (D).

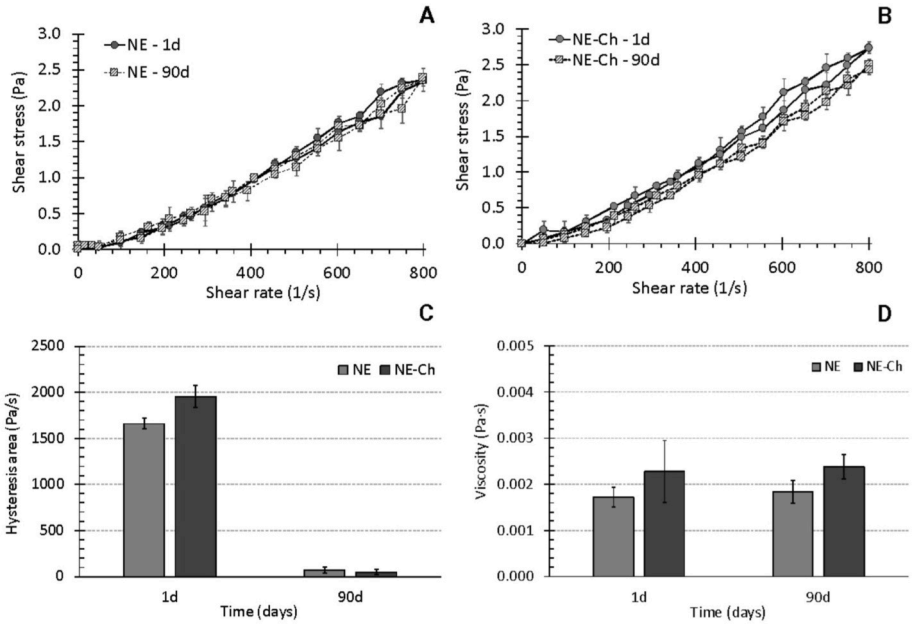

Fig. 8. Rheology of NE and NE-Ch after 1 day (1d) and 3 months (90d). Flow curves (A and B), hysteresis area (C) and apparent viscosities at 250 s-1, upward curve (D). Mean ± standard deviation of n = 3.

aggregation [45,46]. The presence of chitosan coating, which was previously confirmed by ζ-Pot, is visible in Fig. 7 (panel B, C and D), where the nanoparticles spheres were embedded in a rosary-like structure. Moreover, the TEM study demonstrated that intimate contact between Ch-NE and clay particles (PS9 or VHS) is established (panels C and D) and that the NE droplets are homogeneously distributed in the clay (Fig. S5).

3.4. Rheology

The rheology profiles of NE and NE-Ch are shown in Fig. 8. The flow curves of NE showed a non-Newtonian, slightly dilatant profile. The

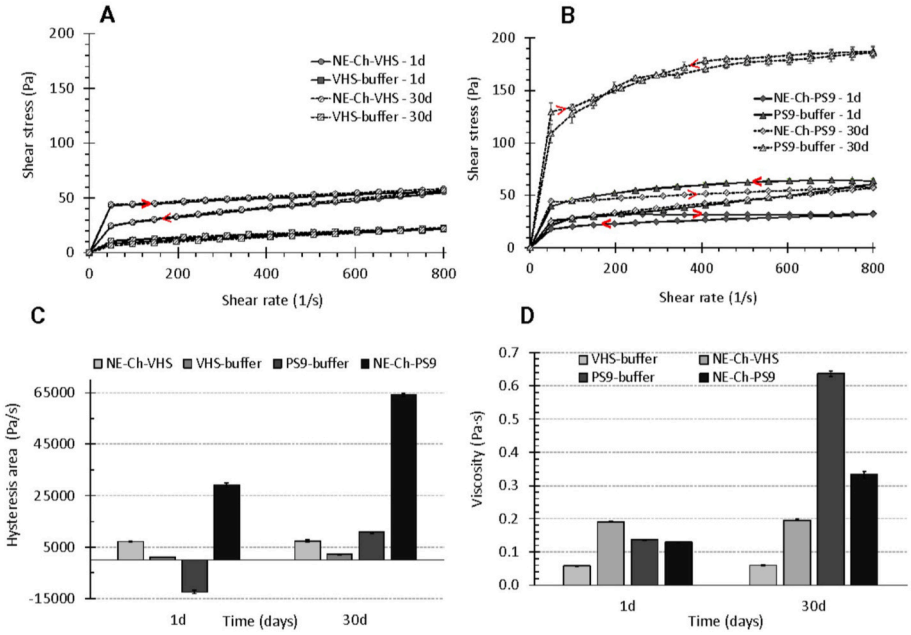

Fig. 9. Rheology of NE-Ch-VHS, NE-Ch-PS9, VHS-buffer and PS9-buffer after 1 and 30 days of preparation. Flow curves (A and B), hysteresis area (C) and apparent viscosities at 250 s-1, upward curve (D). Mean ± standard deviation of n = 3. Red arrows indicate the direction of the flow curves.
In terms of time stability and quality control, formulation with VHS (NE-Ch-VHS) showed the most consistent rheological properties over one month. Despite the fact that the time-evolution of NE-Ch-PS9 is favorable for the formulation (higher viscosity and thixotropy), the uncontrollable nature of these changes could hinder the performance and the quality of the final product. (For interpretation of the references to colour in this figure legend, the reader is referred to the Web version of this article.)

same profile (though with slightly higher apparent viscosity) was shown by NE-Ch, thus meaning that the addition of chitosan did not change the rheological profile of the NE. In this situation, very close to a Newtonian profile, very small interactions occur between particles in the internal structure of the system under stress conditions. As it is widely known, emulsions can present a Newtonian character at low concentrations of the dispersed phase, the non-Newtonian character reported above certain concentrations. Moreover, droplets repel from each other due to their ζ-potential (negative in NE and positive in NE-Ch), also explaining the absence of strong interactions in the system. The slightly higher apparent viscosity of NE-Ch versus NE (more noticeable at 90 days) could be related to differences in droplet sizes: the addition of chitosan increases the diameter (Fig. 3) and, therefore, emulsion droplets are more prone to interact with each other during the application of an external stress. Moreover, as shown by the microscopy (Fig. 7), chitosan addition implies the aggregation of some droplets. Bigger aggregates are more prone to interact with each other, thus explaining the differences between NE and NE-Ch viscosities [47]. Despite being very small, the thixotropic behavior of NE and NE-Ch shown by the positive hysteresis area (Fig. 8, panel C) is a desirable feature for formulations intended to be topically applied. As time passed, the reduction of the hysteresis area (90 days) indicated that the system is more prone to an instantaneous recovery from the stress applied. Nevertheless, the low viscosity values (Fig. 8, panel D), even after the addition of chitosan, is a clear representative of formulation wateriness, thus hindering their administration.

The addition of VHS and PS9 introduced remarkable changes in the rheological properties of NE-Ch (Fig. 9). The corresponding flow curves (Fig. 9, panel A and B) showed non-Newtonian, pseudoplastic profiles. In comparison with their counterparts NE and NE-Ch, the addition of 0.1 g/mL of clay mineral (either VHS or PS9) significantly increased the viscosity of the formulation, thus facilitating its topical administration and improving the stability of the formulation with time. Clay mineral particles possessed higher dimensions with respect to emulsion droplets (Fig. 7), which explains the influence of this ingredient in the rheological properties of the system. Moreover, it is also widely known that clay particles are able to interact with each other in flocculated systems by the establishment of face-to-edge, face-to-face and/or edge-to-edge interactions, depending on factors like medium composition and pH. These interactions also explain the non-Newtonian rheology profiles of clays and their higher consistency. Both NE-Ch-VHS and NE-Ch-PS9 showed thixotropic behavior (Fig. 9, C). VHS-buffer maintained constant rheological properties after 1 month (flow curve, hysteresis area and apparent viscosity), which was extensible to NE-Ch-VHS. On the other hand, the presence of PS9 in NE-Ch induced time changes (Fig. 9). According to the PS9-buffer evolution, the remarkable increase in rheological attributes of NE-Ch-PS9 can be ascribed to the presence of the clay mineral in the formulation. The anti-thixotropic profile of PS9-buffer (1 day, Fig. 9, panel C) was in agreement with previous semisolid formulations based on sepiolite [48]. It is well-known that semisolid systems with acicular/fibrous particles in the internal structure tend towards anti-thixotropic profiles due to the structuration of the system during the application of an external stress. Neaman and Singer stated that coagulated fibrous clay minerals suspensions showed thixotropic behavior, while anti-thixotropic profiles are shown in a dispersed state [49]. According to the present results, it is possible to state that effective interaction between PS9 and NE-Ch was established. That is, the presence of NE-Ch hindered the structuration of PS9 fibers during the application of external stress (shear rate), thus allowing the system to easily flow.

3.5. pH analysis

The degree of acidity and alkalinity are important parameters in skin formulations. In fact, their pH can influence drug/active compound absorption and could induce skin irritation. Many researchers have studied the pH values for topic products, which usually range between 5.0 and 8.0, depending on the ingredients used [50]. In particular, products for skin disease treatment with too extreme pH values can alter the skin surface and trigger trans epidermal water loss, leading to skin irritation [51].

Table 3
pH values of NE, NE-Ch, NE-Ch-VHS, NE-Ch-PS9, VHS and PS9. Values represent the mean ± standard deviation of n = 3 sample measurements.

Sample	pH ± SD
NE	7.26 ± 0.10
NE-Ch	5.13 ± 0.10
VHS	6.87 ± 0.10
PS9	6.73 ± 0.10
NE-Ch-VHS	6.80 ± 0.20
NE-Ch-PS9	6.30 ± 0.10

The pH values of NE, NE-Ch, NE-Ch-VHS, NE-Ch-PS9, VHS and PS9 are reported in Table 3.

After all the characterization, the potential formulations for skin treatment will be NE-Ch-VHS and NE-Ch-PS9. According to the obtained results it is possible to conclude that their pH values are within the recommended pH range (5.5–8.0) [52]. Moreover, it is possible to observe that the inclusion of NE and NE-Ch (pH of 7.26 and 5.13, respectively) inside the clay minerals (VHS and PS9 with respectively pH of 6.87 and 6.73) does not significantly influence the intrinsic pH value of VHS and PS9. Anyway, all the prepared samples have acceptable pH values for skin application.

3.6. In vitro cell studies

3.6.1. Cell biocompatibility and morphology

The biocompatibility of the formulations and their respective pristine components was studied on fibroblasts, the main cells involved in the regulation of ECM protein production [53]. The results reveal that highly concentrated samples show a significant decrease in cell viability. These findings could be ascribed to the presence of particles in suspension that could physically impair gas and nutrient exchanges, leading to a decrease in cell viability [54]. In addition, highly concentrated nanoemulsions could have a cytotoxic effect due to the high CVR concentration. As evident from literature, carvacrol has prominent cytotoxic and apoptotic effects on cells in a dose-dependent manner due to induction of oxidative stress inside the cells [55].

However, considering the dilution 1:200 in DMEM, all samples showed viability percentages higher than 80 % and were superimposable to the positive control (GM), suggesting a biocompatibility in line with the ISO guideline (ISO 10,993 part 5) [56].

To verify that the nanoemulsions were also able to allow normal cell growth, a CLSM analysis of fibroblasts was carried out after 24 h of contact with the samples (1:200 dilution). Fig. 10 (bottom panel) reports the CLSM images of fibroblasts after 24 h contact with the samples (NE, NE-Ch, NE-Ch-VHS, NE-Ch-PS9). Cells nuclei are reported in blue, while cytoskeletons are visible in green (Scale bar: 50 μm). The images confirm the biocompatibility and viability data for all the systems since fibroblasts maintain their normal morphology while in contact with the NE. In fact, all fibroblasts grew uniformly with excellent spread ability all over the well plate surface and were able to reach confluence. The complementary information from the biocompatibility and CLSM results indicates that the developed nanohybrid NE are cell friendly and

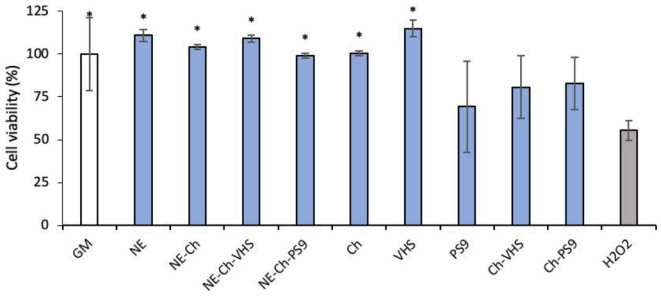

Fig. 11. Fibroblasts cell viability after cell treatment with the samples (diluted 1:200 v/v in DMEM) for 24 h and, then, with H2O2 (1.15 mM) for other 3 h. Cells subjected to the oxidative stress in absence of the samples were considered as control (GM) (mean values ± s.d.; n = 4). * Indicates significant differences ($p < 0.05$) respect to the negative control H2O2.

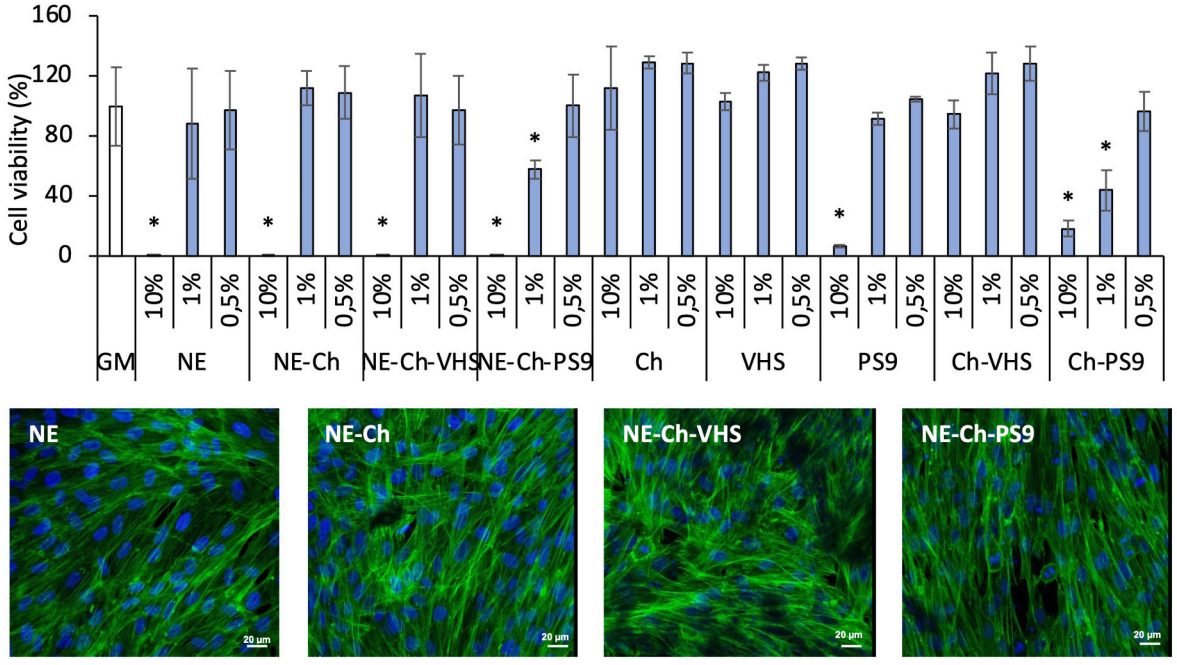

Fig. 10. Fibroblasts cell viability (top panel) after contact with the samples (NE, NE-Ch, NE-Ch-VHS, NE-Ch-PS9) and with the pristine components (Ch, VHS, PS9, Ch-VHS, Ch-PS9) for 24 h (mean values ± s.d.; n = 7) - * indicates significant differences ($p < 0.05$) respect to the control GM; CLSM images of fibroblasts (bottom panel) after contact with the samples (NE, NE-Ch, NE-Ch-VHS, NE-Ch-PS9) for 24 h – in blue: nuclei; in green: cytoskeletons (Scale bar: 50 μm). (For interpretation of the references to colour in this figure legend, the reader is referred to the Web version of this article.)

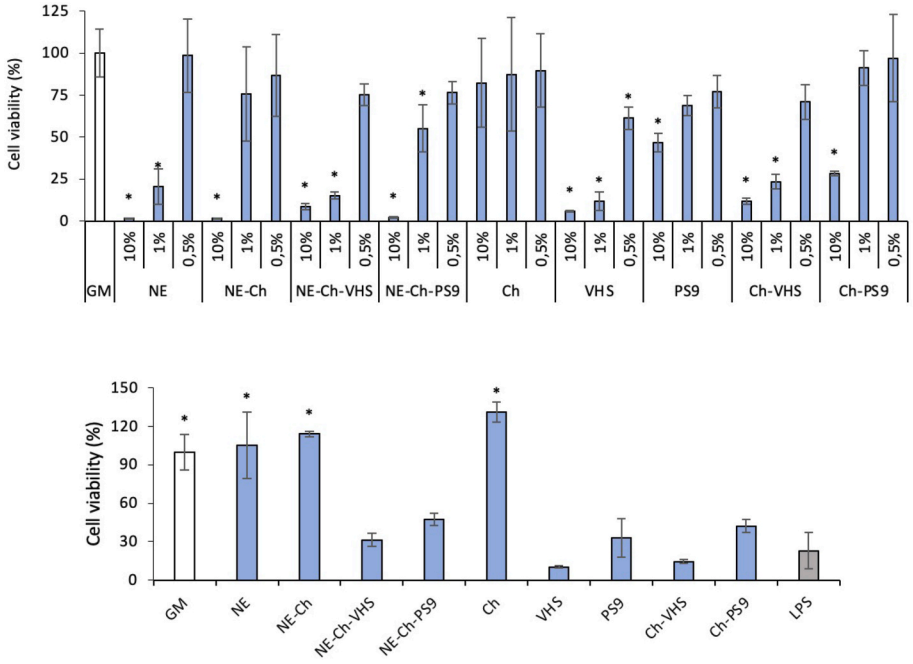

Fig. 12. Macrophages cell viability (top panel) after contact with the samples (NE, NE-Ch, NE-Ch-VHS, NE-Ch-PS9) and with the pristine components (Ch, VHS, PS9, Ch-VHS, Ch-PS9) for 24 h (mean values ± s.d.; n = 5) - * indicates significant differences ($p < 0.05$) respect to the control GM; macrophages cell viability (bottom panel) cell treatment with the samples (diluted 1:200 v/v in DMEM) for 24 h and, then, with LPS solution (1 μg/mL) for other 3 h. Cells subjected to LPS-inflammation in absence of samples were considered as the negative control (LPS). GM, cells grown in standard conditions, was used as reference (mean values ± s.d.; n = 3). * Indicates significant differences ($p < 0.05$) respect to the negative control LPS.

biocompatible.

3.6.2. Assessment of antioxidant properties

Fig. 11 shows fibroblasts cell viability after with the samples (diluted 1:200 v/v in DMEM) for 24 h and then, with H_2O_2 for other 3 h. Preliminary studies (data not shown) indicated that 1.15 mM H_2O_2 was the optimal concentration to cause a proper oxidative damage without complete cell death (about 50 % of cell viability). Therefore, fibroblasts were pre-treated with the samples (1:200 dilution in DMEM) for 24 h and then exposed to oxidative stress with H_2O_2 at 1.15 mM. The results clearly indicate that the nanoemulsions have an antioxidant effect *in vitro*, since they cell viability percentages are comparable to GM (negative control of cells without H_2O_2 treatment) and significantly higher to H_2O_2 (positive control, cells exposed only to H_2O_2 without samples).

Interestingly, Ch and VHS seem to have a key role in determining the antioxidant properties of nanoemulsions. In particular, Ch antioxidant activity is related to its strong hydrogen donation ability, and it has been reported that the lower the molecular weight (less than 150 kDa), the greater the antioxidant activity [57–59]. On the other hand, the antioxidant activity of VHS could be related to the surface absorption of H_2O_2 that could exert a stabilizing effect over hydrogen peroxide, avoiding oxygen reduction. In fact, some researchers have already reported that the presence of clay minerals can exert a synergistic antioxidant effect when combined with other antioxidant molecules [58, 60]. Although there are some contradictory studies, some clay minerals have demonstrated antioxidant activity on their own, mainly ascribable to their chemical composition, the presence of certain metals and to the lack of stability of hydroxyl OH radical species on the clay surface [58, 61,62].

3.6.3. Biocompatibility and anti-inflammatory properties on macrophages

In accordance with the biocompatibility results on fibroblasts, highly concentrated samples reveal a decrease in macrophages cell viability, while samples diluted 1:200 in DMEM show viability percentages superimposable to the positive control.

The anti-inflammatory properties of the samples were studied after macrophages inflammation with lipopolysaccharide (1 μg/ml), an endotoxin that causes rapid cellular responses on macrophages [63]. Fig. 12 (bottom panel) shows cell viability percentages of not inflamed cells (GM), inflamed cells untreated (LPS) and inflamed cells treated with the formulations and their pristine components. NE and NE-Ch nanoemulsions were characterized by a significant anti-inflammatory activity, showing a potential protective effect in LPS-induced murine macrophage cells. This activity could be related to the presence of carvacrol, reported as able to exert anti-inflammatory effects through inhibition of IL-6 production via the ERK1/2 signaling pathway [64]. In addition, Ch also reveals a marked anti-inflammatory activity due to its ability to reduce the expression of interleukins and tumor necrosis factor alpha (TNF-α) [65].

4. Conclusion

Despite its promising properties in wound treatment, CRV exhibits high lipophilicity, rapid oxidation, volatilization, and inadequate retention time at the application site, which limit its therapeutic uses. The current study could represent a brilliant spark for the creation of new hybrid systems, NEs with clays, for the topical application of CRV as a wound healing treatment.

The CRV based NEs proposed in this study and formed by Tw80, coated and uncoated with Ch, showed small hydrodynamic size, homogenous size distribution and stability over time. TEM analyses revealed that all the nanoemulsion samples were almost spherical in shape, the TEM dimensions in agreement with the dimension range obtained by DLS measurements.

The addition of clay minerals (sepiolite and montmorillonite) did not affect the characteristics of the nanodrops in terms of shape and size and they improved the rheological properties of the final formulation.

The *in vitro* biological assays proved that the nanoemulsions were biocompatible towards fibroblasts and macrophages. Moreover, they

exerted antioxidant and anti-inflammatory effects *in vitro*. In view of these results, the proposed nanoemulsions demonstrated to be a good alternative for the topical administration of actives such as CVR, enabling to take advantage of their therapeutic activities to address conditions such as chronic wounds.

Funding

This work has been funded by the European Union - NextGenerationEU under the Italian Ministry of University and Research (MUR) National Innovation Ecosystem grant ECS00000041-Vitality. We acknowledge Università degli Studi di Perugia and MUR for support within the project Vitality.

CRediT authorship contribution statement

Anna Imbriano: Writing – original draft, Visualization, Resources, Methodology, Investigation, Formal analysis, Data curation, Conceptualization. **Fatima García-Villén:** Writing – original draft, Visualization, Resources, Methodology, Investigation, Formal analysis, Conceptualization. **Jacopo Forte:** Writing – original draft, Visualization, Methodology, Investigation, Formal analysis, Data curation, Conceptualization. **Marco Ruggeri:** Writing – original draft, Visualization, Methodology, Investigation, Formal analysis, Data curation, Conceptualization. **Alba Lasalvia:** Visualization, Resources, Methodology, Investigation, Formal analysis, Data curation. **Federica Rinaldi:** Writing – review & editing, Writing – original draft, Visualization, Validation, Supervision, Resources, Methodology, Investigation, Formal analysis, Data curation, Conceptualization. **Luana Perioli:** Supervision, Investigation, Funding acquisition, Conceptualization. **Giuseppina Sandri:** Writing – review & editing, Writing – original draft, Visualization, Validation, Supervision, Resources, Methodology, Investigation, Formal analysis, Conceptualization. **Carlotta Marianecci:** Writing – review & editing, Writing – original draft, Validation, Supervision, Investigation, Formal analysis, Data curation, Conceptualization. **Cesar Viseras:** Writing – review & editing, Validation, Supervision, Resources, Methodology, Investigation, Formal analysis, Conceptualization. **Maria Carafa:** Writing – review & editing, Validation, Supervision, Resources, Methodology, Investigation, Formal analysis, Data curation, Conceptualization.

Declaration of competing interest

The authors declare that they have no known competing financial interests or personal relationships that could have appeared to influence the work reported in this paper.

This work has not been published previously, it is not under consideration for publication elsewhere, its publication is approved by all authors and tacitly or explicitly by the responsible authorities where the work was carried out, and that, if accepted, it will not be published elsewhere in the same form, in English or in any other language, including electronically without the written consent of the copyright-holder.

Data availability

Data will be made available on request.

Appendix A. Supplementary data

Supplementary data to this article can be found online at https://doi.org/10.1016/j.jddst.2024.105984.

References

[1] J.M. Abdo, N.A. Sopko, S.M. Milner, The applied anatomy of human skin: a model for regeneration, Wound Medicine 28 (2020) 100179, https://doi.org/10.1016/j.wndm.2020.100179.
[2] J.M. Benítez, F.J. Montáns, The mechanical behavior of skin: structures and models for the finite element analysis, Comput. Struct. 190 (2017) 75–107, https://doi.org/10.1016/j.compstruc.2017.05.003.
[3] S. Tate, K. Harding, Chronic wound healing, in: Therapeutic Dressings and Wound Healing Applications, John Wiley & Sons, Ltd, 2020, pp. 1–19, https://doi.org/10.1002/9781119433316.ch1.
[4] O. Garraud, W.N. Hozzein, G. Badr, Wound healing: time to look for intelligent, 'natural' immunological approaches? BMC Immunol. 18 (2017) 23, https://doi.org/10.1186/s12865-017-0207-y.
[5] M. Ashtikar, M.G. Wacker, Nanopharmaceuticals for wound healing – lost in translation? Adv. Drug Deliv. Rev. 129 (2018) 194–218, https://doi.org/10.1016/j.addr.2018.03.005.
[6] J.D. Whitney, Overview: acute and chronic wounds, Nursing Clinics 40 (2005) 191–205, https://doi.org/10.1016/j.cnur.2004.09.002.
[7] A. Omar, J.B. Wright, G. Schultz, R. Burrell, P. Nadworny, Microbial biofilms and chronic wounds, Microorganisms 5 (2017) 9, https://doi.org/10.3390/microorganisms5010009.
[8] J. Boateng, O. Catanzano, Advanced therapeutic dressings for effective wound healing—a review, J. Pharmaceut. Sci. 104 (2015) 3653–3680, https://doi.org/10.1002/jps.24610.
[9] A. Fikru, E. Makonnen, T. Eguale, A. Debella, G. Abie Mekonnen, Evaluation of in vivo wound healing activity of methanol extract of Achyranthes aspera L, J. Ethnopharmacol. 143 (2012) 469–474, https://doi.org/10.1016/j.jep.2012.06.049.
[10] B.S. Shetty, Research and reviews: journal of medical and health sciences wound healing and indigenous drugs: role as antioxidants, Review 2 (2013).
[11] M.F. Costa, A.O. Durço, T.K. Rabelo, R.D.S.S. Barreto, A.G. Guimarães, Effects of Carvacrol, Thymol and essential oils containing such monoterpenes on wound healing: a systematic review, J. Pharm. Pharmacol. 71 (2019) 141–155, https://doi.org/10.1111/jphp.13054.
[12] A. Maccelli, L. Vitanza, A. Imbriano, C. Fraschetti, A. Filippi, P. Goldoni, L. Maurizi, M.G. Ammendolia, M.E. Crestoni, S. Fornarini, L. Menghini, M. Carafa, C. Marianecci, C. Longhi, F. Rinaldi, Satureja montana L. Essential Oils, Chemical profiles/phytochemical screening, antimicrobial activity and O/W NanoEmulsion formulations, Pharmaceutics 12 (2020) 7, https://doi.org/10.3390/pharmaceutics12010007.
[13] M.Y. Günal, A. Okçu Heper, N. Zaloğlu, The effects of topical carvacrol application on wound healing process in male rats, Phcog. J. 6 (3) (2014) 10–14, https://doi.org/10.5530/pj.2014.3.2.
[14] M. da S. Lima, L.J. Quintans-Júnior, W.A. de Santana, C. Martins Kaneto, M. B. Pereira Soares, C.F. Villarreal, Anti-inflammatory effects of carvacrol: evidence for a key role of interleukin-10, Eur. J. Pharmacol. 699 (2013) 112–117, https://doi.org/10.1016/j.ejphar.2012.11.040.
[15] J.G. Galvão, R.L. Santos, A.R.S.T. Silva, J.S. Santos, A.M.B. Costa, H. Chandasana, V.V. Andrade-Neto, E.C. Torres-Santos, A.A.M. Lira, S. Dolabella, R. Scher, P. E. Kima, H. Derendorf, R.S. Nunes, Carvacrol loaded nanostructured lipid carriers as a promising parenteral formulation for leishmaniasis treatment, Eur. J. Pharmaceut. Sci. 150 (2020) 105335, https://doi.org/10.1016/j.ejps.2020.105335.
[16] F. Rinaldi, P.N. Hanieh, C. Longhi, S. Carradori, D. Secci, G. Zengin, M. G. Ammendolia, E. Mattia, E. Del Favero, C. Marianecci, M. Carafa, Neem oil nanoemulsions: characterisation and antioxidant activity, J. Enzym. Inhib. Med. Chem. 32 (2017) 1265–1273, https://doi.org/10.1080/14756366.2017.1378190.
[17] D. Julian McClements, Nanoemulsions versus microemulsions: terminology, differences, and similarities, Soft Matter 8 (2012) 1719–1729, https://doi.org/10.1039/C2SM06903B.
[18] P. Sengupta, B. Chatterjee, Potential and future scope of nanoemulgel formulation for topical delivery of lipophilic drugs, Int. J. Pharm. 526 (2017) 353–365, https://doi.org/10.1016/j.ijpharm.2017.04.068.
[19] C. Viseras, C. Aguzzi, P. Cerezo, A. Lopez-Galindo, Uses of clay minerals in semisolid health care and therapeutic products, Appl. Clay Sci. 36 (2007) 37–50, https://doi.org/10.1016/j.clay.2006.07.006.
[20] R. Shemesh, D. Goldman, M. Krepker, Y. Danin-Poleg, Y. Kashi, A. Vaxman, E. Segal, LDPE/Clay/Carvacrol nanocomposites with prolonged antimicrobial activity, J. Appl. Polym. Sci. 132 (2015), https://doi.org/10.1002/app.41261.
[21] C. Viseras, E. Carazo, A. Borrego-Sánchez, F. García-Villén, R. Sánchez-Espejo, P. Cerezo, C. Aguzzi, Clay minerals in skin drug delivery, Clay Clay Miner. 67 (2019) 59–71, https://doi.org/10.1007/s42860-018-0003-7.
[22] F. García-Villén, A. Faccendini, C. Aguzzi, P. Cerezo, M.C. Bonferoni, S. Rossi, P. Grisoli, M. Ruggeri, F. Ferrari, G. Sandri, C. Viseras, Montmorillonite-norfloxacin nanocomposite intended for healing of infected wounds, Int. J. Nanomed. 14 (2019) 5051–5060, https://doi.org/10.2147/IJN.S208713.
[23] I. Khiari, R. Sánchez-Espejo, F. García-Villén, P. Cerezo, C. Aguzzi, A. López-Galindo, F. Jamoussi, C. Viseras, Rheology and cation release of tunisian medina mud-packs intended for topical applications, Appl. Clay Sci. 171 (2019) 110–117, https://doi.org/10.1016/j.clay.2019.01.018.
[24] M.A. Matica, F.L. Aachmann, A. Tøndervik, H. Sletta, V. Ostafe, Chitosan as a wound dressing starting material: antimicrobial properties and mode of action, Int. J. Mol. Sci. 20 (2019) 5889, https://doi.org/10.3390/ijms20235889.
[25] B. Vigani, S. Rossi, G. Sandri, M.C. Bonferoni, C.M. Caramella, F. Ferrari, Hyaluronic acid and chitosan-based nanosystems: a new dressing generation for

wound care, Expet Opin. Drug Deliv. 16 (2019) 715–740, https://doi.org/10.1080/17425247.2019.1634051.
[26] M. Rabišková, J. Valášková, The influence of HLB on the encapsulation of oils by complex coacervation, J. Microencapsul. 15 (1998) 747–751, https://doi.org/10.3109/02652049809008257.
[27] F. Rinaldi, P.N. Hanieh, L.K.N. Chan, L. Angeloni, D. Passeri, M. Rossi, J.T.-W. Wang, A. Imbriano, M. Carafa, C. Marianecci, Chitosan glutamate-coated niosomes: a proposal for nose-to-brain delivery, Pharmaceutics 10 (2018) 38, https://doi.org/10.3390/pharmaceutics10020038.
[28] M. Danaei, M. Dehghankhold, S. Ataei, F. Hasanzadeh Davarani, R. Javanmard, A. Dokhani, S. Khorasani, M.R. Mozafari, Impact of particle size and polydispersity index on the clinical applications of lipidic nanocarrier systems, Pharmaceutics 10 (2018) 57, https://doi.org/10.3390/pharmaceutics10020057.
[29] R.B.I. Mibielli, T. Gerber, L. Mazzarino, M.B. Veleirinho, R.A. Yunes, M. Maraschin, Development of a spectrophotometric method for quantification of carvacrol in nanoemulsions, Revista Brasileira de Farmacognosia 31 (2021), https://doi.org/10.1007/s43450-021-00134-9.
[30] G.B. Martínez-Hernández, M.L. Amodio, G. Colelli, Carvacrol-loaded chitosan nanoparticles maintain quality of fresh-cut carrots, Innovat. Food Sci. Emerg. Technol. 41 (2017) 56–63, https://doi.org/10.1016/j.ifset.2017.02.005.
[31] R.C. de A. Ribeiro, S.M.A.G. Barreto, E.A. Ostrosky, P.A. da Rocha-Filho, L. M. Veríssimo, M. Ferrari, Production and characterization of cosmetic nanoemulsions containing opuntia ficus-indica (L.) mill extract as moisturizing agent, Molecules 20 (2015) 2492–2509, https://doi.org/10.3390/molecules20022492.
[32] R. Aaen, F. Brodin, S. Simon, E. Heggset, K. Syverud, Oil-in-Water emulsions stabilized by cellulose nanofibrils—the effects of ionic strength and pH, Nanomaterials 9 (2019) 259, https://doi.org/10.3390/nano9020259.
[33] K. Dziza, E. Santini, L. Liggieri, E. Jarek, M. Krzan, T. Fischer, F. Ravera, Interfacial properties and emulsification of biocompatible liquid-liquid systems, Coatings 10 (2020) 397, https://doi.org/10.3390/coatings10040397.
[34] Z.E. Suntres, J. Coccimiglio, M. Alipour, The bioactivity and toxicological actions of carvacrol, Crit. Rev. Food Sci. Nutr. 55 (2015) 304–318, https://doi.org/10.1080/10408398.2011.653458.
[35] M.M. Mihai, M.B. Dima, B. Dima, A.M. Holban, Nanomaterials for wound healing and infection control, Materials 12 (2019) 2176, https://doi.org/10.3390/ma12132176.
[36] V.K. Rai, N. Mishra, K.S. Yadav, N.P. Yadav, Nanoemulsion as pharmaceutical carrier for dermal and transdermal drug delivery: formulation development, stability issues, basic considerations and applications, J. Contr. Release 270 (2018) 203–225, https://doi.org/10.1016/j.jconrel.2017.11.049.
[37] E.B. Souto, A.F. Ribeiro, M.I. Ferreira, M.C. Teixeira, A.A.M. Shimojo, J.L. Soriano, B.C. Naveros, A. Durazzo, M. Lucarini, S.B. Souto, A. Santini, New nanotechnologies for the treatment and repair of skin burns infections, Indian J. Manag. Sci. 21 (2020) 393, https://doi.org/10.3390/ijms21020393.
[38] J.-P. Hsu, A. Nacu, Behavior of soybean oil-in-water emulsion stabilized by nonionic surfactant, J. Colloid Interface Sci. 259 (2003) 374–381, https://doi.org/10.1016/S0021-9797(02)00207-2.
[39] A. Gorle, K. Ahire, R. Shende, Design, development and characterization of nanoemulsion developed by high pressure homogenization (HPH) method containing antifungal drug, J. Drug Deliv. Therapeut. 12 (2) (2022) 24–32, https://doi.org/10.22270/jddt.v12i2.5245.
[40] R. Vecchione, U. Ciotola, A. Sagliano, P. Bianchini, A. Diaspro, P.A. Netti, Tunable stability of monodisperse secondary O/W nano-emulsions, Nanoscale 6 (2014) 9300, https://doi.org/10.1039/C4NR02273D.
[41] L. Pavoni, D.R. Perinelli, G. Bonacucina, M. Cespi, G.F. Palmieri, An overview of micro- and nanoemulsions as vehicles for essential oils: formulation, preparation and stability, Nanomaterials 10 (2020) 135, https://doi.org/10.3390/nano10010135.
[42] I.B. Ivanov, P.A. Kralchevsky, Stability of emulsions under equilibrium and dynamic conditions, Colloids Surf. A Physicochem. Eng. Asp. 128 (1997) 155–175, https://doi.org/10.1016/S0927-7757(96)03903-9.
[43] J.M.M. De Oca-Ávalos, R.J. Candal, M.L. Herrera, Nanoemulsions: stability and physical properties, Curr. Opin. Food Sci. 16 (2017) 1–6, https://doi.org/10.1016/j.cofs.2017.06.003.
[44] T.J. Wooster, M. Golding, P. Sanguansri, Impact of oil type on nanoemulsion formation and Ostwald ripening stability, Langmuir 24 (2008) 12758–12765, https://doi.org/10.1021/la801685v.
[45] N. Maisto, D. Mango, A. Bettucci, G. Barbato, M.G. Ammendolia, F. Rinaldi, C. Marianecci, R. Nisticò, M. Carafa, FUS and surfactant-based nanocarriers: a combined strategy for nose to brain drug delivery, J. Drug Deliv. Sci. Technol. 90 (2023) 104977, https://doi.org/10.1016/j.jddst.2023.104977.
[46] F. Rinaldi, J. Forte, G. Pontecorvi, P.N. Hanieh, A. Carè, M. Bellenghi, V. Tirelli, M. G. Ammendolia, G. Mattia, C. Marianecci, R. Puglisi, M. Carafa, pH-responsive oleic acid based nanocarriers: melanoma treatment strategies, Int. J. Pharm. 613 (2022) 121391, https://doi.org/10.1016/j.ijpharm.2021.121391.
[47] Z. Izadiyan, M. Basri, H.R. Fard Masoumi, R. Abedi Karjiban, N. Salim, K. Shameli, Modeling and optimization of nanoemulsion containing Sorafenib for cancer treatment by response surface methodology, Chem. Cent. J. 11 (2017) 21, https://doi.org/10.1186/s13065-017-0248-6.
[48] R.M. Aman, I.I. Abu Hashim, M.M. Meshali, Novel clove essential oil nanoemulgel tailored by taguchi's model and scaffold-based nanofibers: phytopharmaceuticals with promising potential as cyclooxygenase-2 inhibitors in external inflammation, IJN 15 (2020) 2171–2195, https://doi.org/10.2147/IJN.S246601.
[49] M. Ochowiak, L. Broniarz-Press, J. Rozanski, Rheology and structure of emulsions and suspensions, J. Dispersion Sci. Technol. 33 (2012) 177–184, https://doi.org/10.1080/01932691.2010.548694.
[50] F. García-Villén, R. Sánchez-Espejo, A. López-Galindo, P. Cerezo, C. Viseras, Design and characterization of spring water hydrogels with natural inorganic excipients, Appl. Clay Sci. 197 (2020) 105772, https://doi.org/10.1016/j.clay.2020.105772.
[51] D. Indriati, I.Y. Wiendarlina, A.S. Carolina, Formulation and evaluation of anti-acne lotion containing red ginger (zingiber officinalle roscoe) essential oil, Pharmacology and Clinical Pharmacy Research 3 (2018) 61–65, https://doi.org/10.15416/pcpr.v3i3.19841.
[52] N. Matman, Y. Min Oo, T. Amnuaikit, K. Somnuk, Continuous production of nanoemulsion for skincare product using a 3D-printed rotor-stator hydrodynamic cavitation reactor, Ultrason. Sonochem. 83 (2022) 105926, https://doi.org/10.1016/j.ultsonch.2022.105926.
[53] V.V.S.R. Karri, G. Kuppusamy, S.V. Talluri, S.S. Mannemala, R. Kollipara, A. D. Wadhwani, S. Mulukutla, K.R.S. Raju, R. Malayandi, Curcumin loaded chitosan nanoparticles impregnated into collagen-alginate scaffolds for diabetic wound healing, Int. J. Biol. Macromol. 93 (2016) 1519–1529, https://doi.org/10.1016/j.ijbiomac.2016.05.038.
[54] M. Ruggeri, E. Bianchi, B. Vigani, R. Sánchez-Espejo, M. Spano, C. Totaro Fila, L. Mannina, C. Viseras, S. Rossi, G. Sandri, Nutritional and functional properties of novel Italian spray-dried cricket powder, Antioxidants 12 (2023) 112, https://doi.org/10.3390/antiox12010112.
[55] I. Khan, A. Bahuguna, P. Kumar, V.K. Bajpai, S.C. Kang, In vitro and in vivo antitumor potential of carvacrol nanoemulsion against human lung adenocarcinoma A549 cells via mitochondrial mediated apoptosis, Sci. Rep. 8 (2018) 144, https://doi.org/10.1038/s41598-017-18644-9.
[56] W. Li, J. Zhou, Y. Xu, Study of the in vitro cytotoxicity testing of medical devices, Biomedical Reports 3 (2015) 617–620, https://doi.org/10.3892/br.2015.481.
[57] J. Vinsova, E. Vavrikova, Chitosan derivatives with antimicrobial, antitumour and antioxidant activities - a review, CPD 17 (2011) 3596–3607, https://doi.org/10.2174/138161211798194468.
[58] M. M, N. Raghavendra, N.R. Bhumika, C.H. Chaithra, B.N. Nagalaxmi, K. N. Shravana Kumara, Study of ZnO nanoparticle-supported clay minerals for electrochemical sensors, photocatalysis, and antioxidant applications, ChemPhysMater 3 (2024) 83–93, https://doi.org/10.1016/j.chphma.2023.07.002.
[59] C. Gonçalves, N. Ferreira, L. Lourenço, Production of low molecular weight chitosan and chitooligosaccharides (COS): a review, Polymers 13 (2021) 2466, https://doi.org/10.3390/polym13152466.
[60] S. Li, B. Mu, H. Zhang, Y. Kang, A. Wang, Incorporation of silver nanoparticles/curcumin/clay minerals into chitosan film for enhancing mechanical properties, antioxidant and antibacterial activity, Int. J. Biol. Macromol. 223 (2022) 779–789, https://doi.org/10.1016/j.ijbiomac.2022.11.046.
[61] J. Cervini-Silva, A. Nieto-Camacho, V. Gómez-Vidales, Oxidative stress inhibition and oxidant activity by fibrous clays, Colloids Surf. B Biointerfaces 133 (2015) 32–35, https://doi.org/10.1016/j.colsurfb.2015.05.042.
[62] J. García-Tojal, E. Iriarte, S. Palmero, M.R. Pedrosa, C. Rad, S. Sanllorente, M. C. Zuluaga, M. Cavia-Saiz, D. Rivero-Perez, P. Muñiz, Phyllosilicate-content influence on the spectroscopic properties and antioxidant capacity of Iberian Cretaceous clays, Spectrochim. Acta Mol. Biomol. Spectrosc. 251 (2021) 119472, https://doi.org/10.1016/j.saa.2021.119472.
[63] N. Somensi, T.K. Rabelo, A.G. Guimarães, L.J. Quintans-Junior, A.A. de Souza Araújo, J.C.F. Moreira, D.P. Gelain, Carvacrol suppresses LPS-induced pro-inflammatory activation in RAW 264.7 macrophages through ERK1/2 and NF-kB pathway, Int. Immunopharm. 75 (2019) 105743, https://doi.org/10.1016/j.intimp.2019.105743.
[64] C. Yan, W. Kuang, L. Jin, R. Wang, L. Niu, C. Xie, J. Ding, Y. Liao, L. Wang, H. Wan, G. Ma, Carvacrol protects mice against LPS-induced sepsis and attenuates inflammatory response in macrophages by modulating the ERK1/2 pathway, Sci. Rep. 13 (2023) 12809, https://doi.org/10.1038/s41598-023-39665-7.
[65] A. Madni, R. Kousar, N. Naeem, F. Wahid, Recent advancements in applications of chitosan-based biomaterials for skin tissue engineering, Journal of Bioresources and Bioproducts 6 (2021) 11–25, https://doi.org/10.1016/j.jobab.2021.01.002.